

12

Best Available Copy

AD-A167 665

OFFICE OF NAVAL RESEARCH

CONTRACT NO. N00014-84-C-0723

INTERIM TECHNICAL REPORT 0001AF

CHARACTERIZATION OF ILLUMINATED SEMICONDUCTOR/
SOLID-ELECTROLYTE JUNCTIONS
SEMICONDUCTOR REDOX POLYMER DETECTOR JUNCTIONS

By

Sharon K. Schmidt, Ronald L. Cook and Anthony F. Sammells

Accepted for publication in

THE JOURNAL OF THE ELECTROCHEMICAL SOCIETY

September 15, 1985

ELTRON RESEARCH, INC.
4260 Westbrook Dr.
Aurora, IL 60505

DTIC
SELECTED
MAY 13 1988
S D

Reproduction in whole or in part is permitted for any purpose of the United States Government.

This document has been approved for public release and sale; its distribution is unlimited.

20030121068

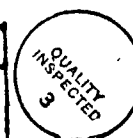
DTIC FILE COPY

REPORT DOCUMENTATION PAGE		READ INSTRUCTIONS BEFORE COMPLETING FORM
1. REPORT NUMBER 0001AF	2. GOVT ACCESSION NO.	3. RECIPIENT'S CATALOG NUMBER
4. TITLE (and Subtitle) CHARACTERIZATION OF ILLUMINATED SEMICONDUCTOR/SOLID-ELECTROLYTE JUNCTIONS. SEMICONDUCTOR REDOX POLYMER DETECTOR JUNCTIONS		5. TYPE OF REPORT & PERIOD COVERED Technical July 16, 1985 September 15, 1985
		6. PERFORMING ORG. REPORT NUMBER
7. AUTHOR(s) Sharon K. Schmidt, Ronald L. Cook and Anthony F. Sammells		8. CONTRACT OR GRANT NUMBER(s) N00014-84-C-0723
9. PERFORMING ORGANIZATION NAME AND ADDRESS		10. PROGRAM ELEMENT, PROJECT, TASK AREA & WORK UNIT NUMBERS NR 627-826
11. CONTROLLING OFFICE NAME AND ADDRESS Office of Naval Research/Chemistry Program Arlington, VA 22217		12. REPORT DATE September 15, 1985
		13. NUMBER OF PAGES
14. MONITORING AGENCY NAME & ADDRESS (if different from Controlling Office)		15. SECURITY CLASS. (of this report) Unclassified
		15a. DECLASSIFICATION/DOWNGRADING SCHEDULE
16. DISTRIBUTION STATEMENT (of this Report) Approved for Public Release; Distribution Unlimited		
17. DISTRIBUTION STATEMENT (of the abstract entered in Block 20, if different from Report) Accepted for Publication in THE JOURNAL OF THE ELECTROCHEMICAL SOCIETY		
18. SUPPLEMENTARY NOTES		
19. KEY WORDS (Continue on reverse side if necessary and identify by block number) Nafion 117; n-TiO ₂ ; Solid-State Photoelectrochemical Cells <i>n-type titanium dioxide</i> <i>sub fb</i>		
20. ABSTRACT (Continue on reverse side if necessary and identify by block number) The dependency of n-TiO ₂ flatband potential (V_{fb}) for cells of the general configuration: n-TiO ₂ /Nafion 117, Redox species/SnO ₂ conducting glass, was systematically studied for the redox species Ru(bpy) ₃ ²⁺ , Fe(bpy) ₃ ²⁺ and Ru(NH ₃) ₆ ³⁺ as a function of their concentration within the polymer. The linear relationship $V_{fb} = M(1/\text{concentration}) + b$, was found to hold for all cells. The slope (M) was found dependent upon metal complex used and its oxidation state. The sensitivity of n-TiO ₂ , V_{fb} to its immediate chemical environment at its interface with the redox polymer can be a strategy pursued for chemical detection. <i>Keywords</i>		

TABLE OF CONTENTS

	<u>Page</u>
List of Figures	iv
Table	iv
Experimental	1
Introduction	2
Results and Discussion	3
References	7

Accession For	
NTIS CRA&I	<input checked="" type="checkbox"/>
DTIC TAB	<input type="checkbox"/>
Unannounced	<input type="checkbox"/>
Justification	
By	
Distribution /	
Availability Codes	
Dist	Avail and/or Special
A-1	



LIST OF FIGURES

<u>Figure Numbers</u>	<u>Page</u>
1. Energy level diagram for metal-metal oxide/semiconductor cell, analogy used for SnO ₂ conducting glass/SPE/n-TiO ₂ cells in this study.	8
2. Passive element network for C _{sc} measurement in Mott-Schottky analyses.	9
3. Frequency response of cell n-TiO ₂ /Nafion 117 + 0.00075g/ml Ru(bpy) ₃ ²⁺ /SnO ₂ Cond. Glass at V = 0.04 V vs. SnO ₂ Cond. Glass.	10
4. Frequency response of the cell n-TiO ₂ /Nafion 117 + 0.00075g/ml Ru(bpy) ₃ ²⁺ /SnO ₂ Cond. Glass at V = 0.04 V vs. SnO ₂ Cond. Glass.	11
5. Mott-Schottky plot for the cell n-TiO ₂ /Nafion + NaPF ₆ + Fe(bpy) ₃ ²⁺ /SnO ₂ Conducting Glass.	12
6. Mott-Schottky plot for the cell n-TiO ₂ /Nafion + NaPF ₆ + Ru(bpy) ₃ ²⁺ /SnO ₂ Conducting Glass.	13
7. Mott-Schottky plot for the cell n-TiO ₂ /Nafion + NaPF ₆ +Ru(NH ₃) ₆ ³⁺ /SnO ₂ Conducting Glass.	14
8. Plot of 1/concentration of Fe(bpy) ₃ ²⁺ vs. V _{fb} for the cell n-TiO ₂ /Nafion + NaPF ₆ + Fe(bpy) ₃ ²⁺ /SnO ₂ Conducting Glass.	15
9. Plot of 1/concentration of Ru(bpy) ₃ ²⁺ vs. V _{fb} for the cell n-TiO ₂ /Nafion + NaPF ₆ + Ru(bpy) ₃ ²⁺ /Conducting Glass.	16
10. Plot of 1/concentration of Ru(NH ₃) ₆ ³⁺ vs. V _{fb} for the cell n-TiO ₂ /Nafion + NaPF ₆ + Ru(NH ₃) ₆ ³⁺ /SnO ₂ Conducting Glass.	17
11. Comparison of 1/concentration vs. V _{fb} for the cells n-TiO ₂ /Nafion + Redox Couple + NaPF ₆ /SnO ₂ Conducting Glass for redox species Ru(NH ₃) ₆ ³⁺ , Ru(bpy) ₃ ²⁺ and Fe(bpy) ₃ ²⁺ .	18
12. Plot of V _{fb} for n-TiO ₂ /Nafion, Ru(NH ₃) ₆ ³⁺ interface vs. V _{fb} of n-TiO ₂ /Nafion, Fe(bpy) ₃ ²⁺ interface as a function of the redox concentration incorporated into polymer.	19
13. Plot of V _{fb} for n-TiO ₂ /Nafion, Ru(bpy) ₃ ²⁺ interface vs. V _{fb} of n-TiO ₂ /Nafion, Ru(NH ₃) ₆ ³⁺ interface as a function of the redox concentration incorporated into polymer.	20
14. Plot of V _{fb} for n-TiO ₂ /Nafion, Ru(bpy) ₃ ²⁺ interface vs. V _{fb} of n-TiO ₂ /Nafion, Fe(bpy) ₃ ²⁺ interface as a function of the redox concentration incorporated into polymer.	21

TABLE

Table 1. Flatband potentials as a function of the nature and concentration of the redox species in the cell: n-TiO ₂ /Nafion + NaPF ₆ + Redox species/SnO ₂ cond. glass.	22
--	----

EXPERIMENTAL

Single crystal n-TiO₂ was heated under hydrogen at 800°C for several hours. Ohmic contact to the back surface of the crystal was made by the introduction of gallium-indium eutectic into the freshly etched (c.H₂SO₄) surface. Current collection was accomplished with a nichrome wire and silver epoxy (Epoxy Technology, Inc.), and the assembly cured at 150°C for 1 hour. A 5^w/o Nafion 117 solution in a mixture of lower aliphatic alcohols and 10^w/o water was obtained from Aldrich. Sodium conductivity was introduced into the polymer using NaPF₆. Cells were constructed by placing a drop of exchanged Nafion suspension onto a freshly etched (c.H₂SO₄, 10 seconds) electrode face. A drop of redox-containing polymer was also placed on a SnO₂ conducting glass counter electrode. Both electrodes were dried for approximately 15 minutes, and then the half-cells gently pressed together and allowed to dry for an additional 10 minutes. Electrochemical measurements were performed using potentiostatic control provided by either a Stonehart Associates BC 1200 or a Wenking LT 78 potentiostat. Conductance and capacitance measurements for admittance spectroscopy analysis of the polymer-semiconductor interface were performed using a HP-4276A digital LCZ meter between 100 and 20kHz.

INTRODUCTION

As has been previously discussed by us, there are several incentives for characterizing semiconductor junctions with solid polymer electrolytes (SPE) incorporating redox species. These include 1) the identification of solid-state photoelectrochemically rechargeable galvanic cells which possess some faradaic charge capacity^{1,2}, and 2) the potential role of polymer-incorporated redox couples as antenna probe at the semiconductor surface for the detection of chemical species via the perturbation of a semiconductor parameter such as the flatband potential (V_{fb})³ or surface state density.

We will discuss here the dependency of V_{fb} for n-TiO₂ as a function of concentration for the species Ru(bpy)₃²⁺, Fe(bpy)₃²⁺ and Ru(NH₃)₆³⁺ incorporated into sodium conducting Nafion 117. Typical cells possessed the configuration:



Of interest to us here was the analogy of such SPE cells to MOSFET (Metal-Oxide-Semiconductor Field Effect Transistors) devices which have previously been used for the detection of H₂, C₃H₈, H₂S, NH₃ and EtOH⁴. The detection mechanism used in these latter devices involves the initial dissociation of the species to be detected at a metal catalytic site followed by the migration of atomic hydrogen through the metal to the metal/metal oxide interface region^{5,6}. Here, the adsorbed hydrogen atoms act as dipoles at the interface, thereby changing the metal work function. This dipole layer, in turn, gives rise to an extra voltage in series with an externally applied voltage. Here, the actual change in the work function is assumed to be proportional to the interface concentration of adsorbed hydrogen or the hydrogen coverage. The response of such MOS-type detectors is dependent upon the oxide layer quality. The presence of defects in this region can result in device instability resulting from ion drift or a variable density of interface trap sites. Semiconductor parameters such as V_{fb} can be modified by the nature of the oxide layer and its thickness, dielectric charge and the presence of fixed charges. In the case of silicon-based devices, the flatband potential can be found dependent upon the following parameters:⁷

$$V_{fb} = \phi_m - \chi_s - \frac{E_g}{2} - \phi_f - \frac{W_{ox}}{\epsilon_{ox}} Q_s$$

where ϕ_m is the metal work function, χ_s is the semiconductor electron affinity,

E_g is the semiconductor band gap, ϕ_f is the difference between the semiconductor mid-band and its Fermi level, W_{ox} and ϵ_{ox} are respectively the thickness and dielectric constant of the metal oxide and Q_s is the charge associated with the resident oxide. This last term (Q_s) can, in principle, be adjusted in semiconductor/redox SPE cells investigated here by varying the concentration of redox species incorporated into the SPE.

If these polymer incorporated redox species were to possess some sensitivity to a chemical species to be detected via an appropriate redox mechanism, then the resultant changes in activity by these incorporated species could be determined by measuring changes in V_{fb} . In MOSFET-type devices used for detector applications, performance instabilities can result from defects present in the metal oxide layer⁸. The presence of such defects can result in changes in the charge associated with the metal oxide and introduce trap sites for electron and electron hole carriers. Substitution of the metal oxide by a redox containing polymer at this interface region is one strategy that can be pursued for improving overall device stability. A schematic energy level diagram for an MOS cell is shown in Figure 1 as an approximate analogy for the semiconductor/redox SPE junction of interest here.

The objective of the work reported there was to determine the relationship between frequency independent V_{fb} values for n-TiO₂, at n-TiO₂/redox SPE interface, as a function of the concentration of redox species introduced into the polymer.

RESULTS AND DISCUSSION

Work reported here was directed towards the dependency of V_{fb} for n-TiO₂ in solid-state cells of the configuration:

n-TiO₂/Nafion 117 + NaPF₆ + redox species/SnO₂ conducting glass
as a function of the concentration of the redox species introduced into the SPE. Metal complexes introduced into the Nafion ion exchange sites included Ru(bpy)₃²⁺, Fe(bpy)₃²⁺ and Ru(NH₃)₆³⁺. These complexes were chosen to investigate the relative influence of metal oxidation state (Ru²⁺ vs. Ru³⁺) and metal (Ru²⁺ vs. Fe²⁺) upon the measured flatband potential. Concentrations of redox complex were typically varied between 5 and 1 μ mole/ml of the 5W/o Nafion 117 SPE solution. A limitation in the determination of V_{fb} from impedance or admittance measurements lies in correlating measured parameters with the elements representing the equivalent circuit of the n-TiO₂/redox SPE interface region. Here, the parameters

being measured are based upon resistive or capacitive elements arranged in either a series or parallel configuration as represented in Figure 2. The magnitude of these parameters will be dependent upon the measurement frequency. This is in comparison to the equivalent circuit elements⁹ which are passive and can be used to gain information on surface-state energies and faradaic charge transfer rates, etc. As we have discussed previously, a technique has been developed for the measurement of frequency independent Mott-Schottky parameters¹⁰. This technique was used to obtain Mott-Schottky data from which V_{fb} values for n-TiO₂ at various SPE interface could be determined. For Mott-Schottky analyses conducted here at the n-TiO₂/SPE interface, the passive network element of interest was the space charge capacitance. In this analyses, the double layer capacitance (C_{dl}) was assumed to be much larger than C_{sc} (i.e. $C_{dl} \gg C_{sc}$) although some components of C_{dl} may be present in the measured C_{sc} values. The simplest equivalent circuit configuration of the semiconductor/SPE interface region consists of the space charge capacitance (C_{sc}) connected in series with the bulk conductance G_B ¹¹ (Figure 2). The admittance of this circuit was given by the equation:

$$Y_x = \frac{\omega^2 G_B C_{sc}^2 + j\omega G_B^2 C_{sc}}{G_B^2 + (\omega C_{sc})^2}$$

where ω is the angular frequency ($2\pi f$). The measured parameters, G_p (parallel conductance) and C_p (parallel capacitance) were obtained directly using an HP-4276 LCZ meter. The related admittance was obtained by use of the relationship:¹⁰

$$Y_z = G_p + j \omega C_p$$

Relating the real and imaginary components of Y_x and Y_z gives:

$$C_p/\omega = \frac{\omega C_{sc}^2 G_B}{G_B^2 + (\omega C_{sc})^2}$$

and

$$\omega C_p = \frac{\omega G_B^2 C_{sc}}{G_B^2 + (\omega C_{sc})^2}$$

Plots of G_p/ω vs. ω and ωC_p vs. ω will exhibit maxima at a frequency $\omega_{max} = G_B/C_{sc}$ and the desired parameters C_{sc} and G_B can be obtained through the following relationship:

$$G_p/\omega_{max} = C_{sc}/2$$

and

$$\omega C_{pmax} = G_B/2$$

C_{sc} obtained in this manner is frequency independent and thus a plot of C_{sc} values obtained at varying bias voltages will yield frequency independent Mott-Schottky plots for the determination of V_{fb} .

Figures 3 and 4 show typical G_p/ω vs. ω and ωC_p vs. ω plots for the system $n\text{-TiO}_2/\text{Ru}(\text{bpy})_3^{2+} + \text{NaPF}_6 + \text{Nafion 117}/\text{SnO}_2$ conducting glass. In both of these figures, the solid curve represents the theoretical response, calculated using the model RC circuit and values of R_B and C_{sc} derived from the experimental data. As can be seen from both of these figures, good agreement between experimental and calculated curves was obtained in the middle of the frequency range, around ω_{max} . Discrepancies by the model at lower frequencies may be corrected by the introduction of a resistor corresponding to the faradaic cell conductance. This modification, which would be in parallel with C_{sc} , would affect only the low frequency response and not G_{pmax} . Mott-Schottky data obtained by plotting C_{sc} at each bias potential for the cell:

$n\text{-TiO}_2/\text{Nafion 117} + \text{NaPF}_6 + \text{Redox couple}/\text{SnO}_2$ conducting glass are shown in Figures 5-7 where the redox species were respectively $\text{Fe}(\text{bpy})_3^{2+}$, $\text{Ru}(\text{bpy})_3^{2+}$ and $\text{Ru}(\text{NH}_3)_6^{3+}$. Over the semiconductor bias region studied (0 - 1V vs. SnO_2 conducting glass) these plots exhibited good linearity and the carrier concentrations (N_D) were in reasonable agreement to N_D values obtained from solution measurements in 0.1M H_3PO_4 (i.e. $N_D = 8 \times 10^{19} \text{ cm}^{-3}$).

The flatband values obtained as a function of redox concentration within the SPE are shown in Table 1. As was observed for all complexes introduced into the SPE, V_{fb} was found to shift cathodically with decreasing concentration of redox species. Additionally, $n\text{-TiO}_2$ V_{fb} values were found to be inversely proportional to the concentration of redox species. This observation is illustrated respectively for the redox species $\text{Fe}(\text{bpy})_3^{2+}$, $\text{Ru}(\text{bpy})_3^{2+}$ and $\text{Ru}(\text{NH}_3)_6^{3+}$ in Figures 8-10. All three of these plots are summarized in Figure 11.

Figures 12-14 also show respectively that linear relationships exist when V_{fb} for the $n\text{-TiO}_2/\text{Nafion}$, $\text{Ru}(\text{NH}_3)_6^{3+}$ interface is plotted vs. V_{fb} for $n\text{-TiO}_2/\text{Nafion}$, $\text{Fe}(\text{bpy})_3^{2+}$, V_{fb} for $n\text{-TiO}_2/\text{Nafion}$, $\text{Ru}(\text{bpy})_3^{2+}$ is plotted vs. V_{fb} for $n\text{-TiO}_2/\text{Nafion}$, $\text{Ru}(\text{NH}_3)_6^{3+}$, and V_{fb} for $n\text{-TiO}_2/\text{Nafion}$, $\text{Ru}(\text{bpy})_3^{2+}$ is plotted vs. V_{fb} of $n\text{-TiO}_2$, $\text{Fe}(\text{bpy})_3^{2+}$, all as a function of transition metal complex incorporated into the polymer.

From these observations, it appears that the relationship

$$V_{fb} = M(1/\text{concentration}) + b$$

holds in all cases.

The slope appears to be determined, in part, by the transition metal complex incorporated into the SPE and maybe, more importantly, by its oxidation state. This latter point is graphically illustrated when we compare slopes for $\text{Ru}(\text{NH}_3)_6^{3+}$ and $\text{Ru}(\text{bpy})_3^{2+}$ incorporated polymers (Figure 11). Hence, introduction of polymer incorporated chemically sensitive transition metal complexes into such cells could be used for the detection of chemical species via measuring changes in V_{fb} . These results were found to be completely reproducible. Such observations, however, differ from those that would be expected on an MOS-type device where direct proportionality would be expected between V_{fb} and the fixed charge (Q_s) associated with the oxide layer.

REFERENCES

1. A.F. Sammells and P.G.P. Ang, J. Electrochem. Soc., 131 617 (1984).
2. A.F. Sammells and S.K. Schmidt, J. Electrochem Soc., 132 520 (1985).
3. R.L. Cook and A.F. Sammells, J. Electrochem. Soc., 132 2429 (1985).
4. "Solid State Chemical Sensors," Edited by J. Janata and R.J. Huber, Academic Press (1985).
5. I. Lundström, M.S. Shivaraman and C. Svensson, Surf. Sci., 64 497 (1977).
6. I. Lundström, M.S. Shivaraman and C. Svensson, J. Appl. Phys., 46 3876 (1975).
7. S.M. Sze, "Physics of Semiconductor Devices," Wiley (Interscience), New York, NY (1981).
8. B.E. Deal, J. Electrochem. Soc., 121 198C (1974).
9. V. Del Toro, "Principles of Electrical Engineering," Prentice-Hall, Englewood Cliffs, NJ (1972).
10. J. Dubow and R. Krishnar, "Novel Concepts in Electrochemical Solar Cells," SERI Final Report; Contract #XS-0-9272-1 Oct. (1981).
11. A. Many, V. Goldstein and N.B. Grover, "Semiconductor Surfaces," North Holland, Amsterdam, (1965).

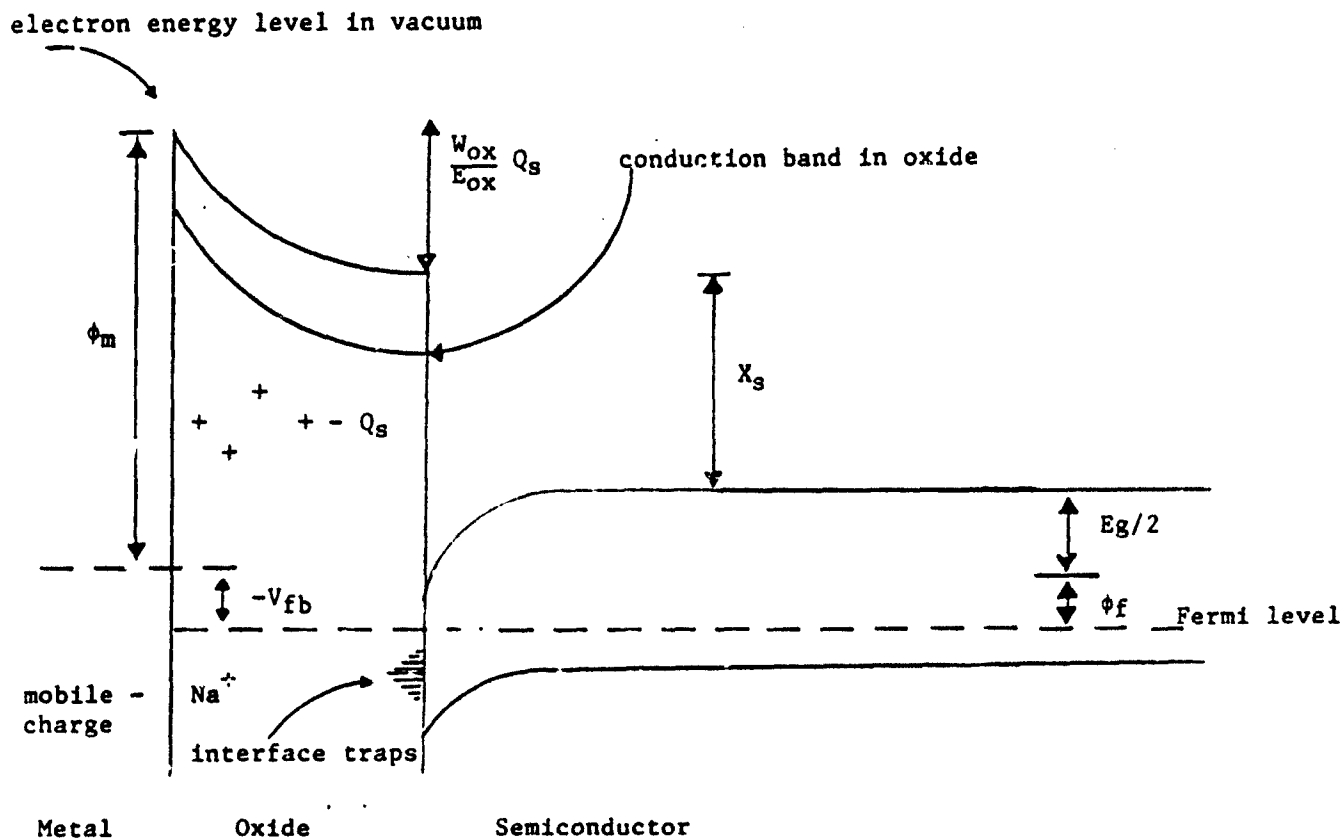


Figure 1. Energy level diagram for metal-metal oxide-semiconductor cell. analogy used for SnO_2 conducting glass/SPE/n- TiO_2 cells in this study.

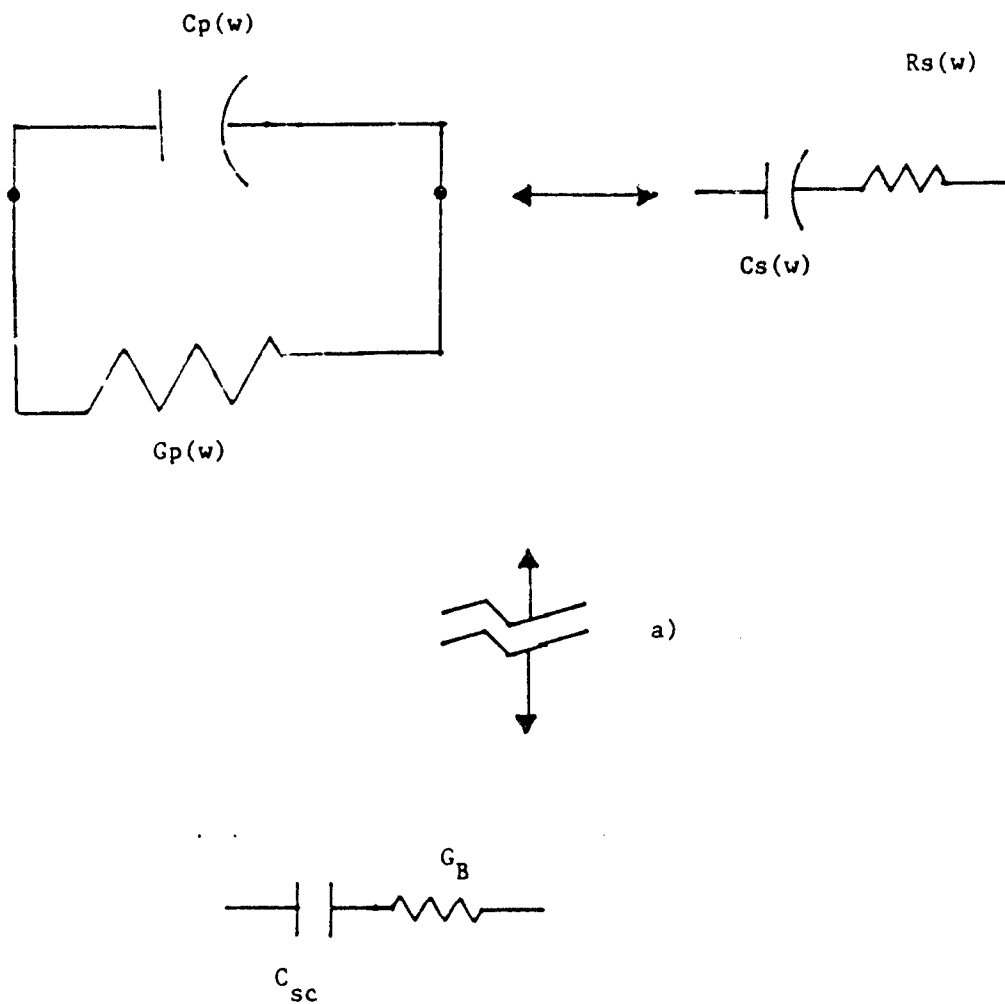


Figure 2. Passive element network for C_{sc} measurement in Mott-Schottky analyses.

- a) This transformation is performed by a successive reduction in the equivalent circuit representation of the semiconductor/SPE interface⁶.

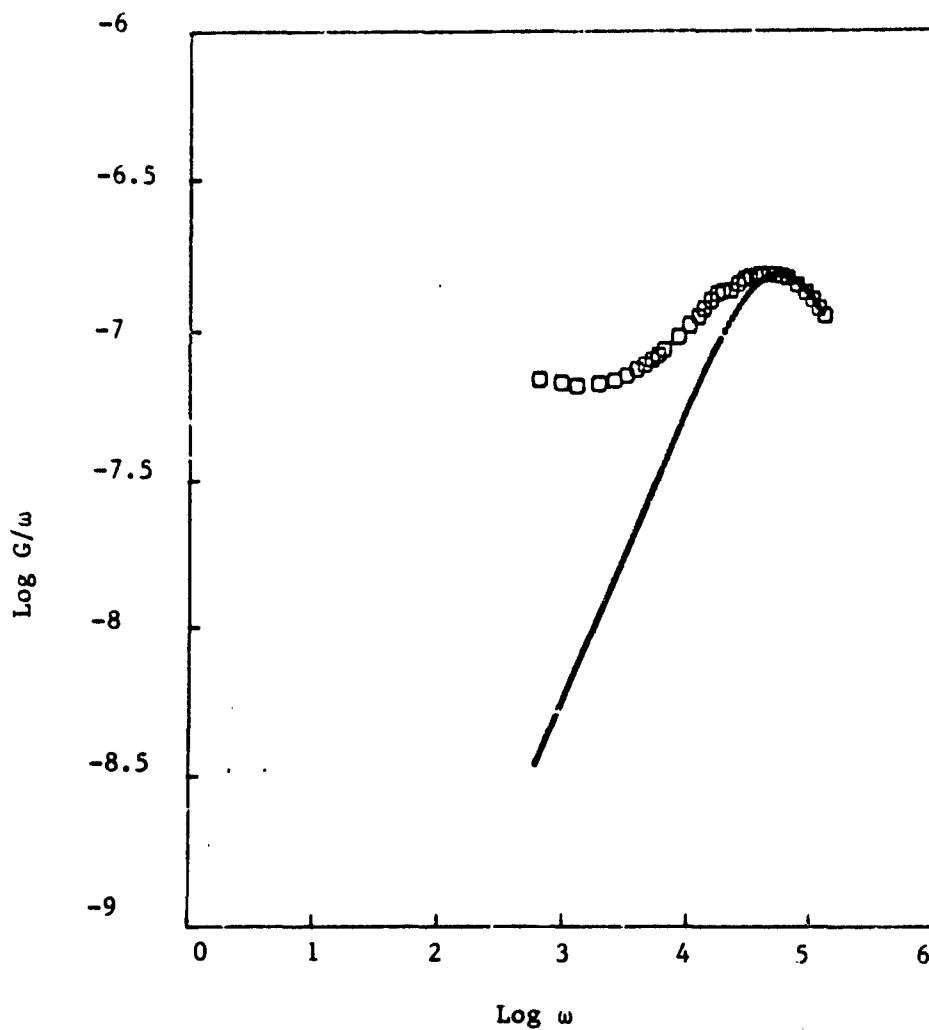


Figure 3. Frequency Response of the Cell
 $n\text{-TiO}_2/\text{Nafion 117} + 0.00075\text{g/ml Ru}(\text{bpy})_3^{2+}/\text{SnO}_2$ Cond. Glass
 at $V = 0.04$ V vs. SnO_2 Cond. Glass
 □ = Experimental Data
 — = Simulation of RC Series Circuit.
 $R_B = 58.5 \Omega$. $C_{sc} = 307.7$ nF

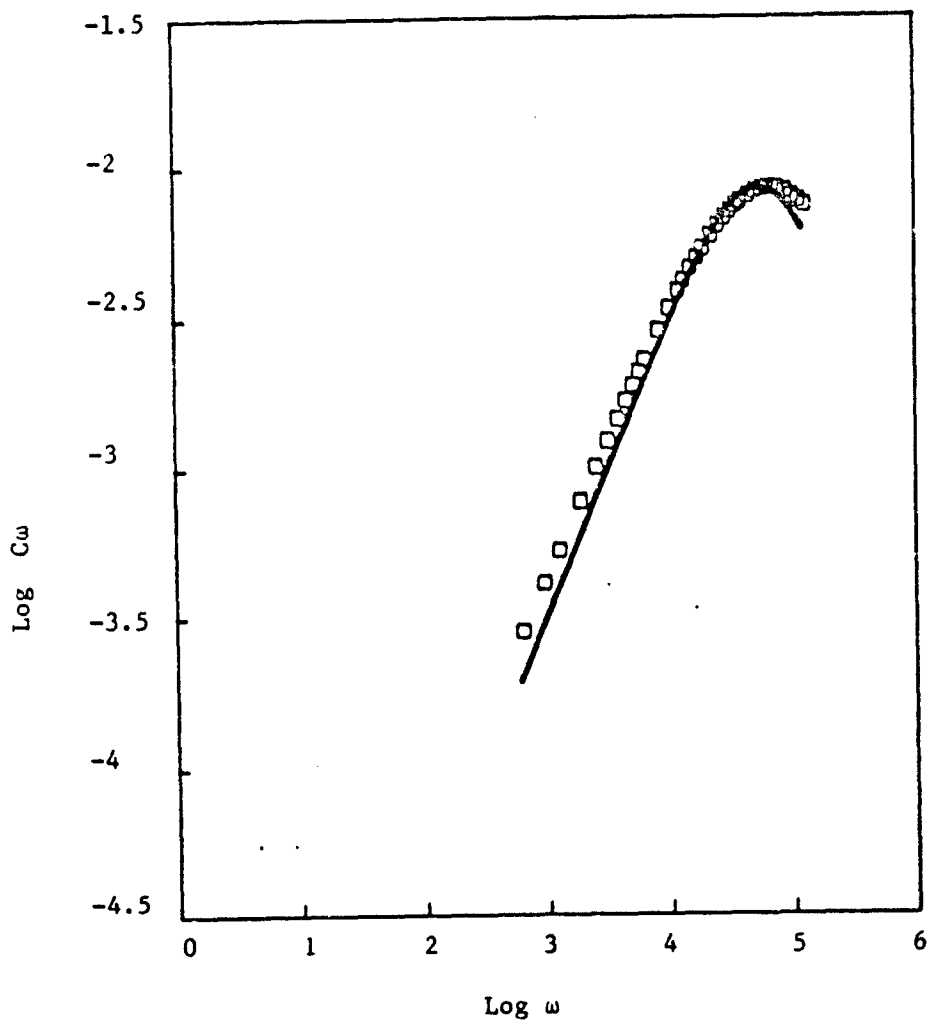


Figure 4. Frequency Response of the Cell
 $n\text{-TiO}_2/\text{Nafion 117} + 0.00075 \text{ g/ml Ru}(\text{bpy})_3^{2+}/\text{SnO}_2 \text{ Cond. Glass}$
 at $V = 0.04 \text{ V vs. SnO}_2 \text{ Cond. Glass}$
 □ = Experimental Data
 — = Simulation of RC Series Circuit.
 $R_B = 58.5 \Omega. C_{sc} = 307.7 \text{ nF.}$

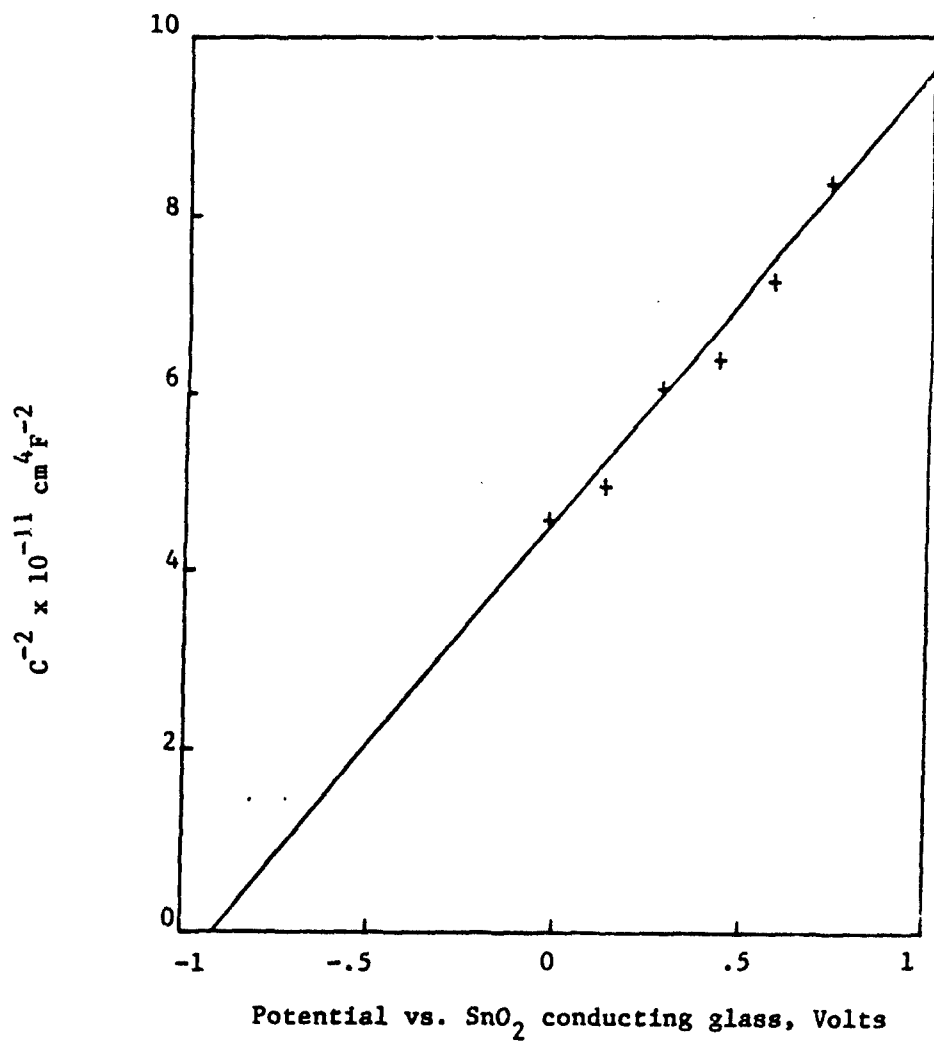


Figure 5. Mott-Schottky plot for the cell
 $n\text{-TiO}_2/\text{Nafion} + \text{NaPF}_6 + \text{Fe}(\text{bpy})_3^{2+}/\text{SnO}_2$ conducting glass
 (.00025 g/ml $\text{Fe}(\text{bpy})_3^{2+}$).

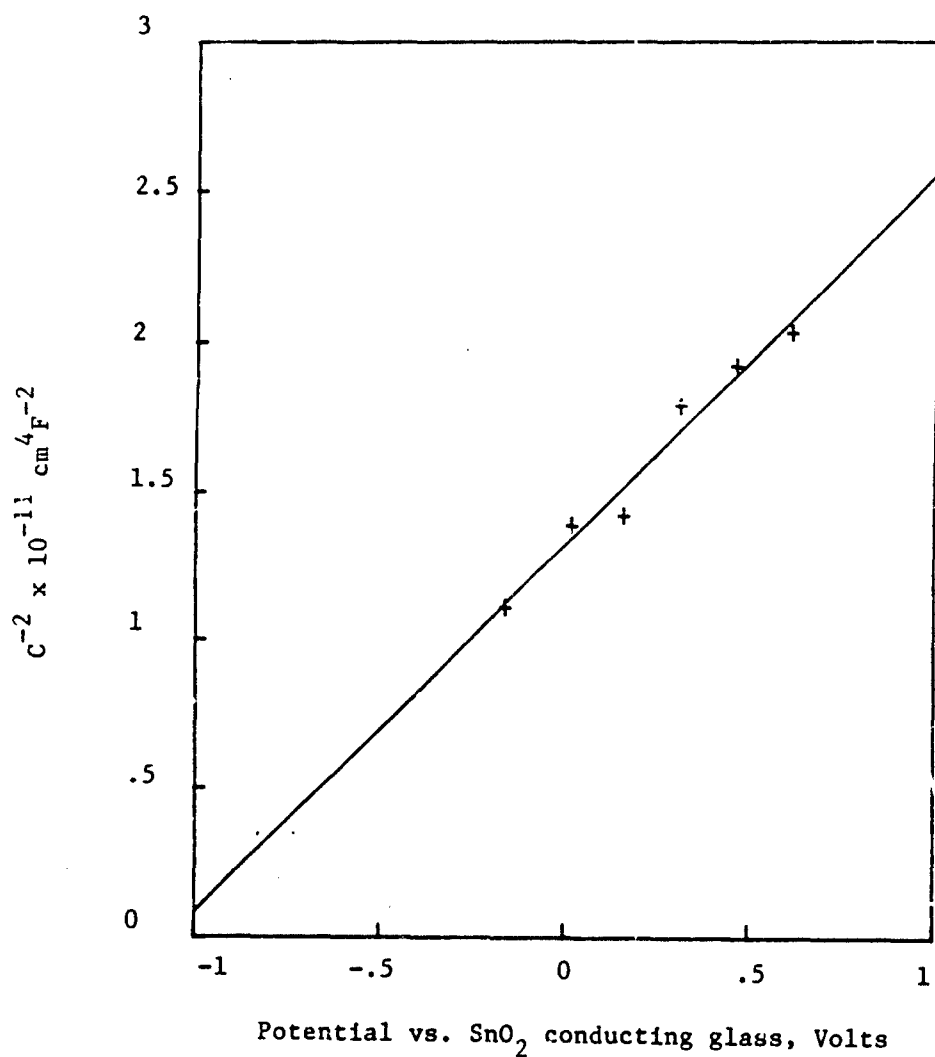


Figure 6. Mott-Schottky plot for the cell
 $n\text{-TiO}_2/\text{Nafion} + \text{NaPF}_6 + \text{Ru}(\text{bpy})_3^{2+}/\text{SnO}_2$ conducting glass
 (.0015 g/ml $\text{Ru}(\text{bpy})_3^{2+}$).

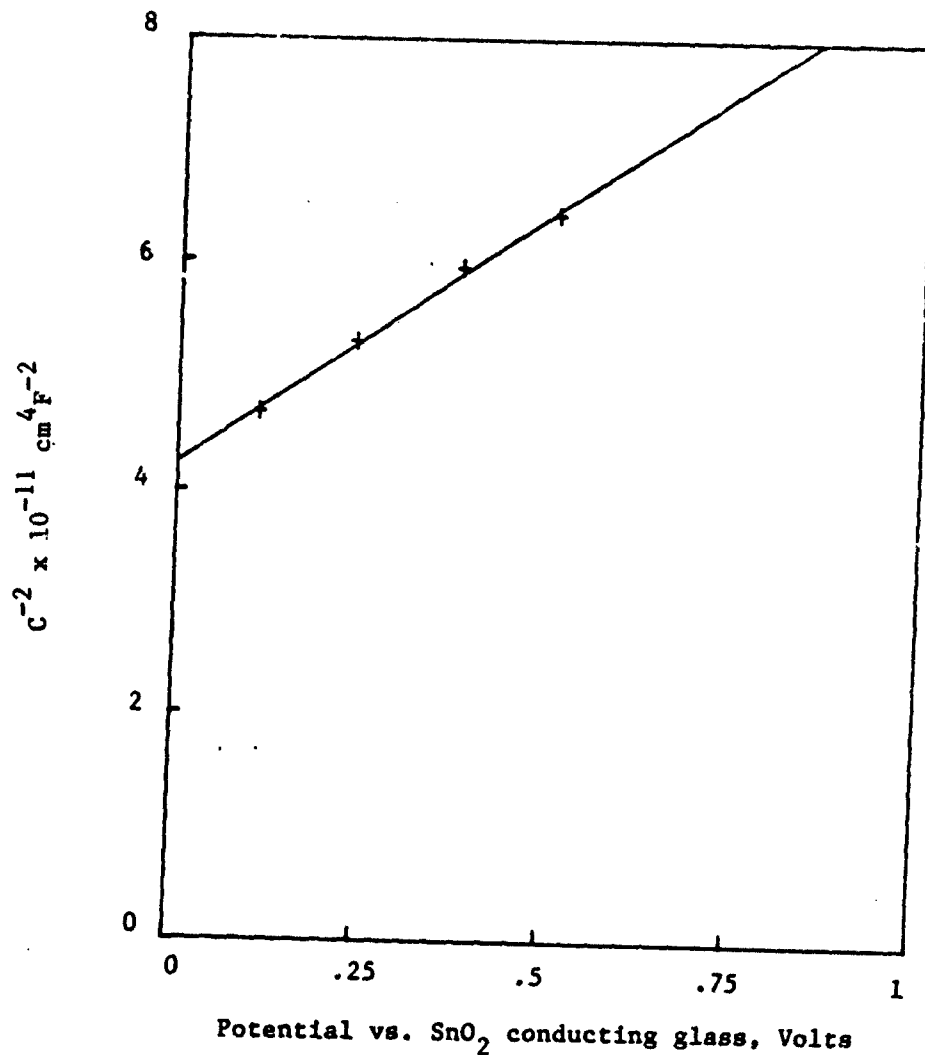


Figure 7. Mott-Schottky plot for the cell
 $n\text{-TiO}_2/\text{Nafion} + \text{NaPF}_6 \text{ Ru}(\text{NH}_3)_6^{3+}/\text{SnO}_2$ conducting glass
 (.000375 g/ml $\text{Ru}(\text{NH}_3)_6^{3+}$).

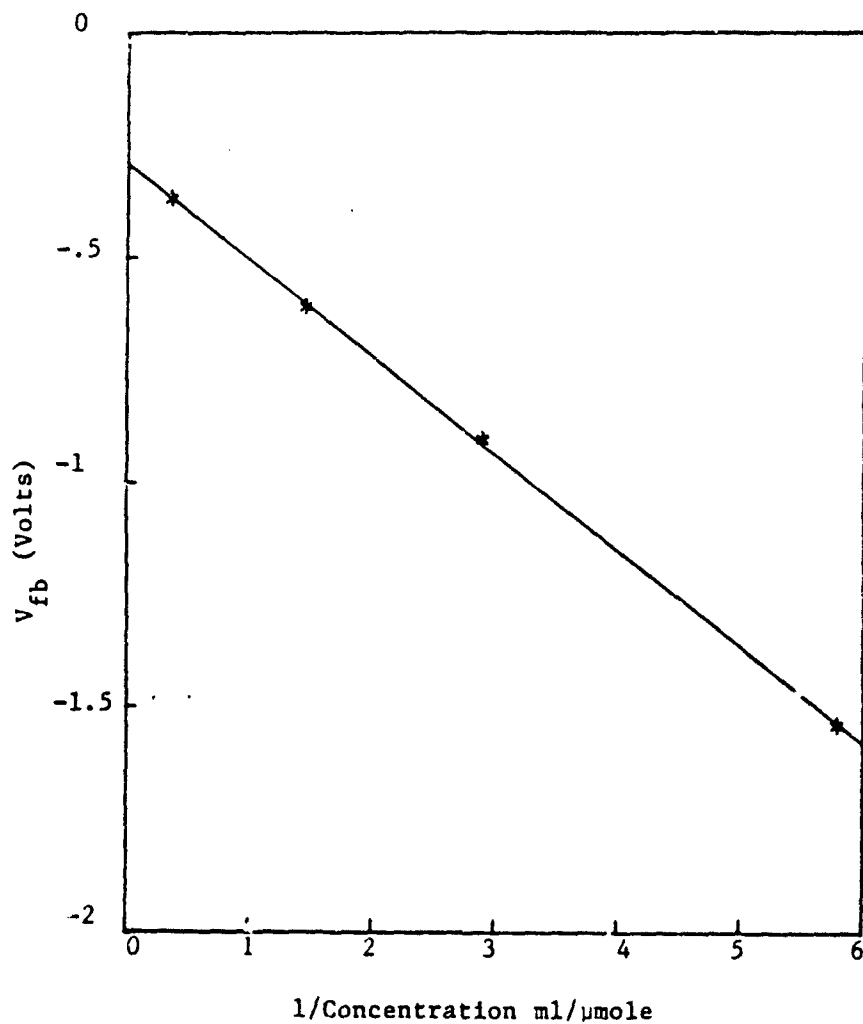


Figure 8. Plot of 1/concentration of $\text{Fe}(\text{bpy})_3^{2+}$ vs. V_{fb} for the cell $\text{n-TiO}_2/\text{Nafion} + \text{NaPF}_6 + \text{Fe}(\text{bpy})_3^{2+}/\text{SnO}_2$ conducting glass.

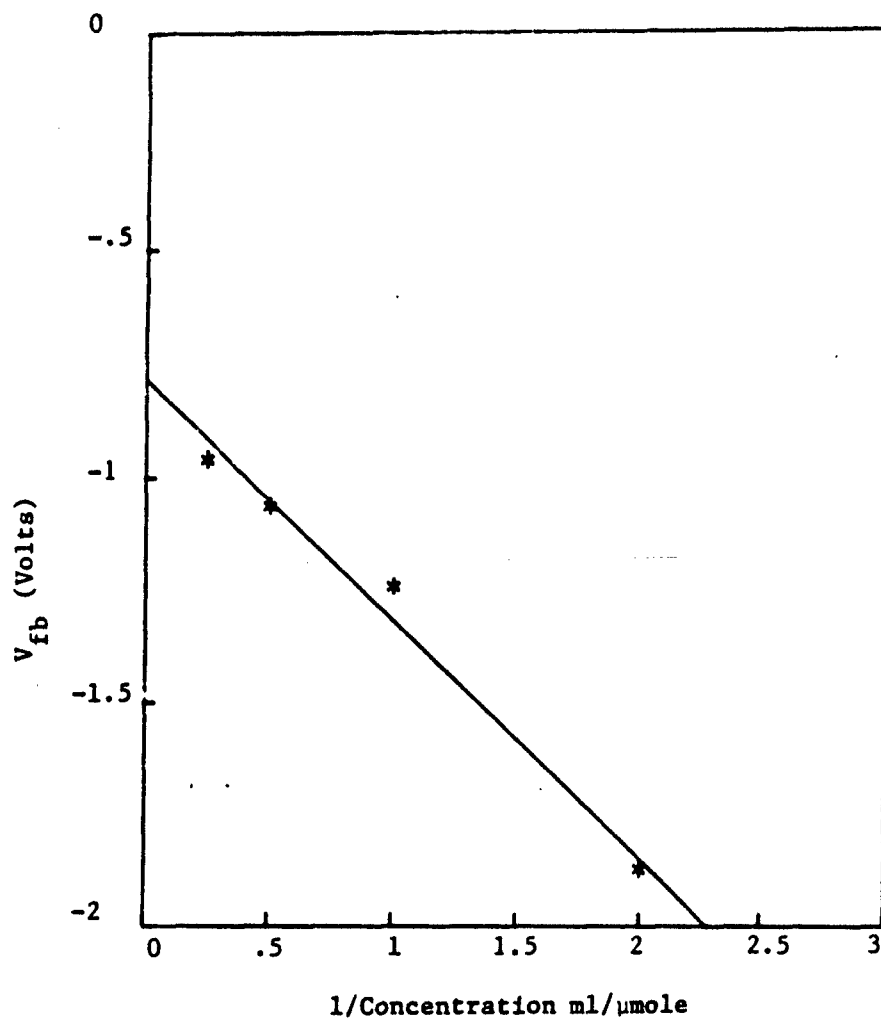


Figure 9. Plot of 1/concentration of $\text{Ru}(\text{bpy})_3^{2+}$ vs. V_{fb} for the cell $n\text{-TiO}_2/\text{Nafion} + \text{NaPF}_6 + \text{Ru}(\text{bpy})_3^{2+}/\text{Conducting glass}$.

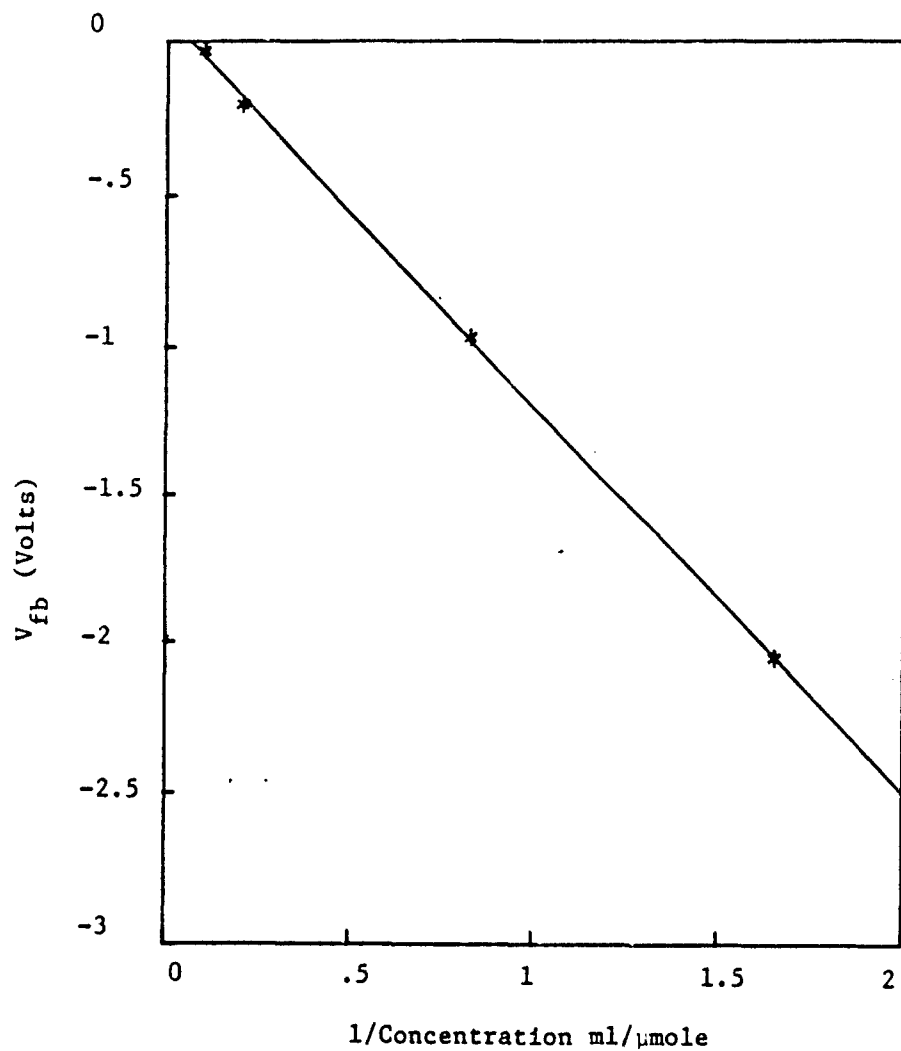


Figure 10. Plot of 1/concentration of $\text{Ru}(\text{NH}_3)_6^{3+}$ vs. V_{fb} for the cell $n\text{-TiO}_2/\text{Nafion} + \text{NaPF}_6 + \text{Ru}(\text{NH}_3)_6^{3+}/\text{SnO}_2$ conducting glass.

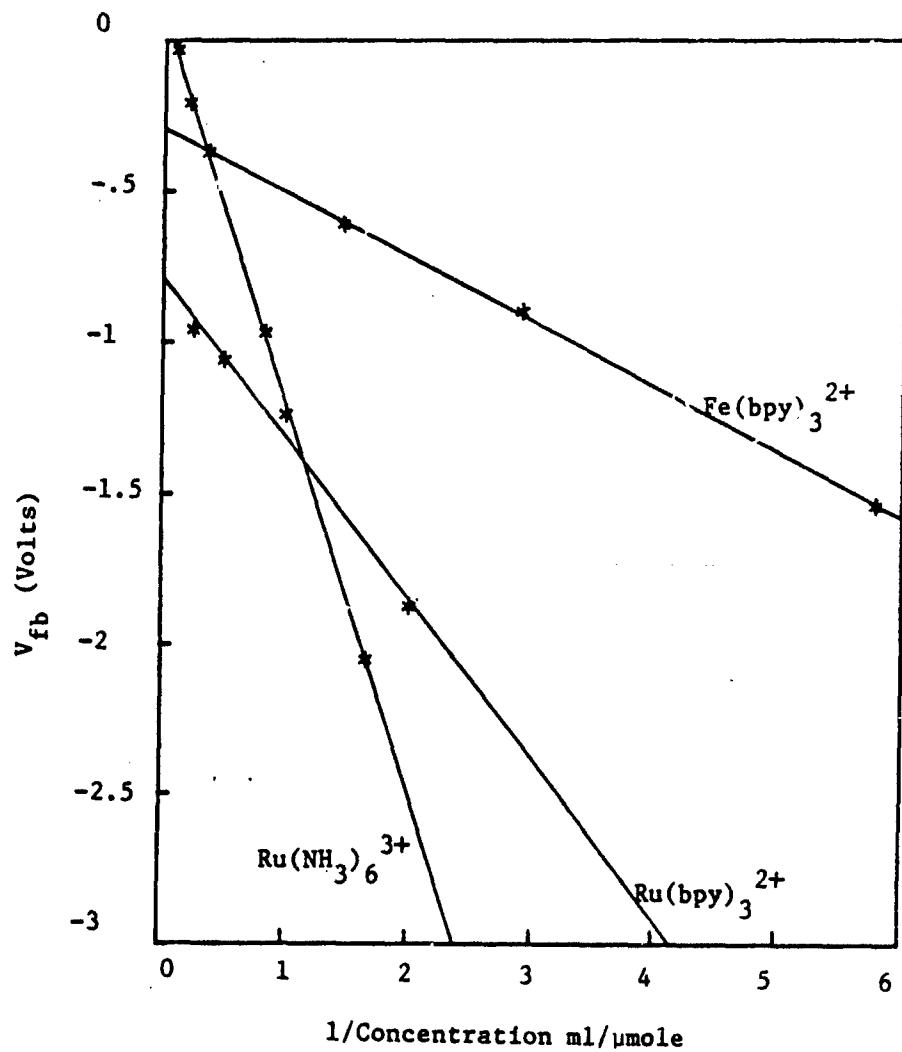


Figure 11. Comparison of 1/concentration vs. V_{fb} for the cells $n\text{-TiO}_2/\text{Nafion} + \text{Redox Couple} + \text{NaPF}_6/\text{Conducting glass}$ for redox species $\text{Ru}(\text{NH}_3)_6^{3+}$, $\text{Ru}(\text{bpy})_3^{2+}$ and $\text{Fe}(\text{bpy})_3^{2+}$.

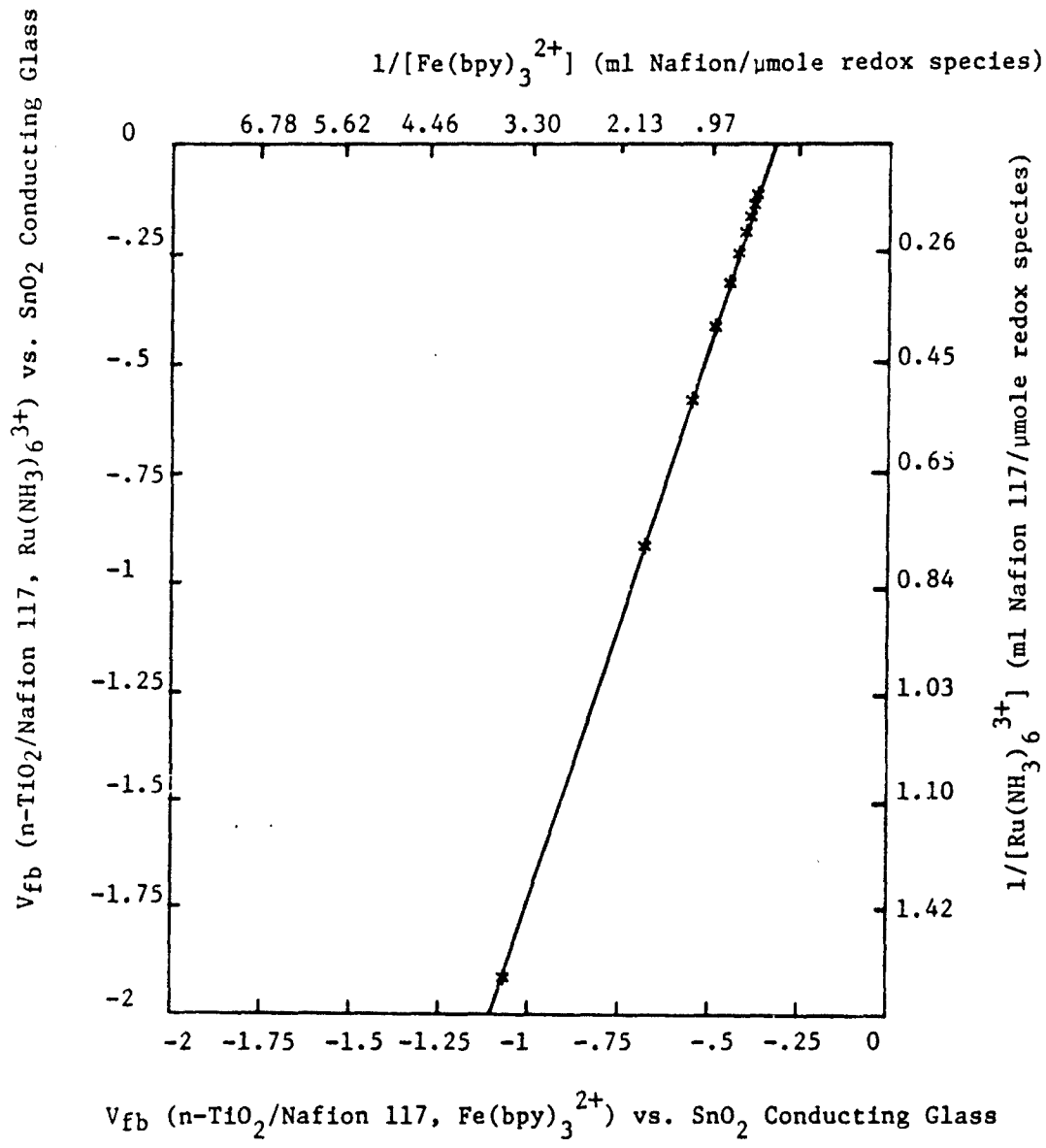


Figure 12. Plot of V_{fb} for n-TiO₂/Nafion, Ru(NH₃)₆³⁺ interface vs. V_{fb} of n-TiO₂/Nafion, Fe(bpy)₃²⁺ interface as a function of the redox concentration incorporated into polymer.

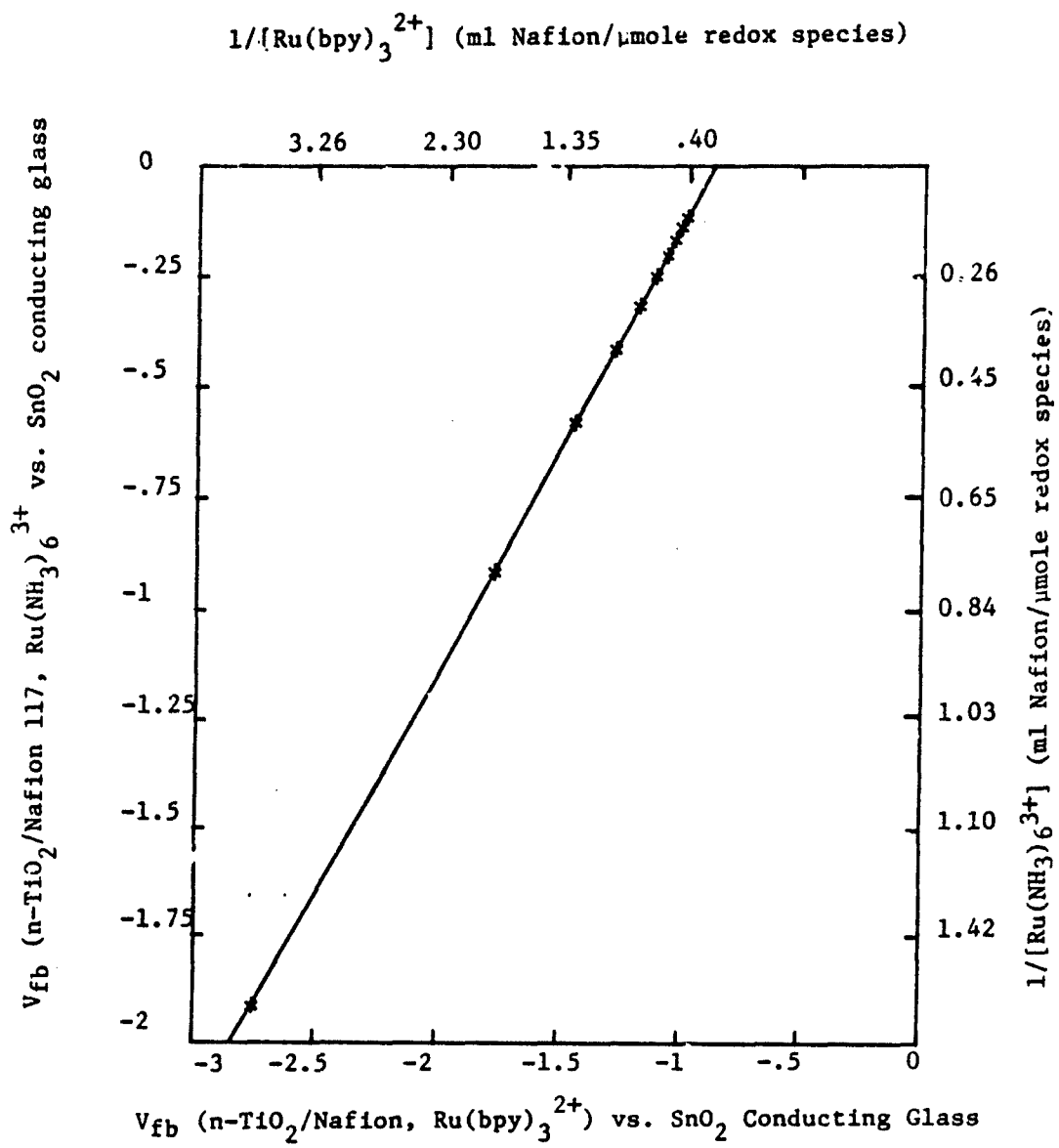


Figure 13. Plot of V_{fb} for n-TiO₂/Nafion, Ru(bpy)₃²⁺ interface vs. V_{fb} of n-TiO₂/Nafion, Ru(NH₃)₆³⁺ interface as a function of the redox concentration incorporated into polymer.

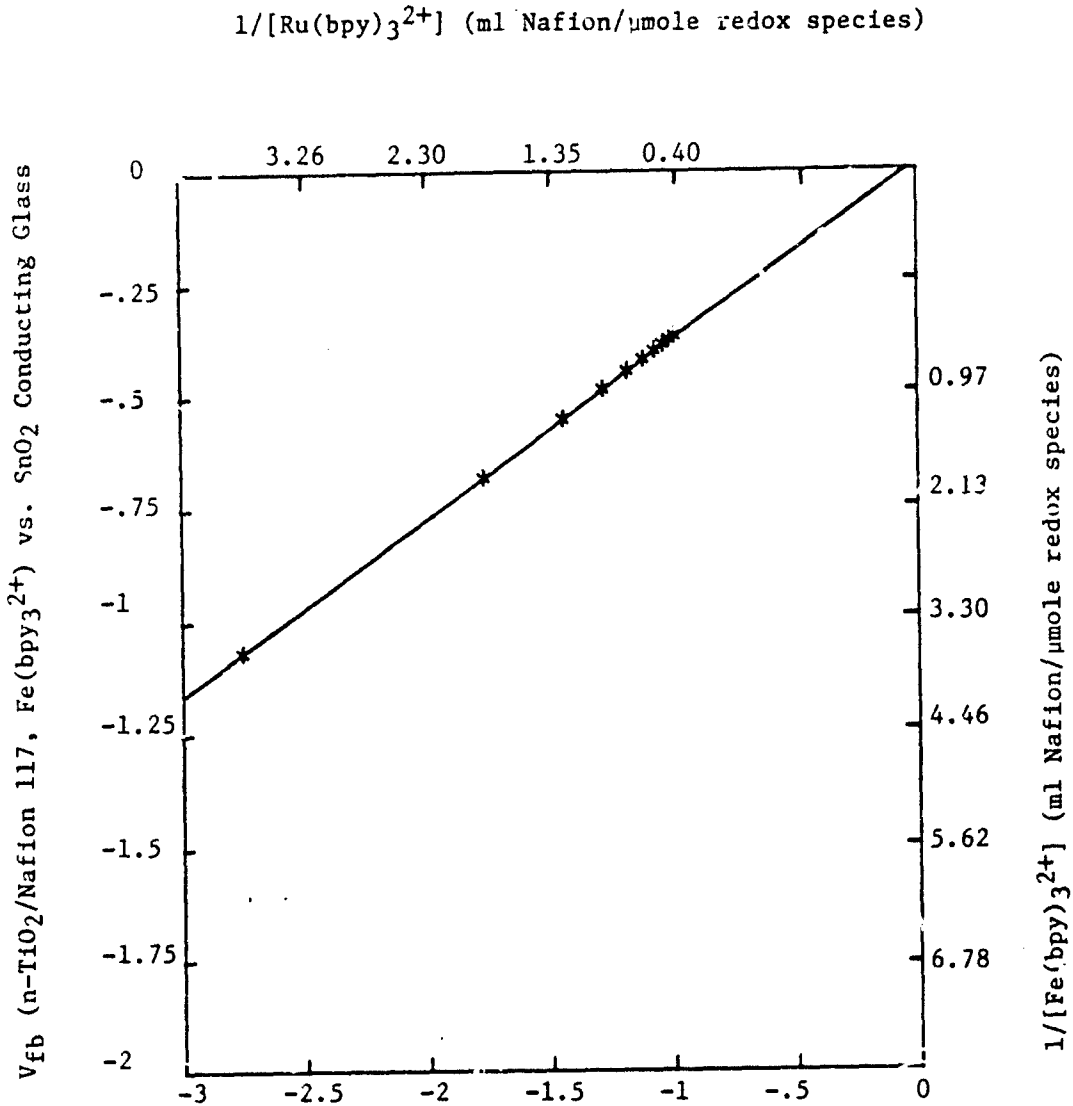


Figure 14. Plot of V_{fb} for n-TiO₂/Nafion, Ru(bpy)₃²⁺ interface vs. V_{fb} of n-TiO₂/Nafion, Fe(bpy)₃²⁺ interface as a function of the redox concentration incorporated into polymer.

Table 1. Flatband potentials as a function of the nature and concentration of the redox species in the cell:

n-TiO₂/Nafion + NaPF₆ + Redox species/SnO₂ conducting glass.

Complex	Concentration (μ mole/ml) ^a	V _{fb}
Fe(bpy) ₃ ²⁺	2.77	-0.37
	0.691	-0.61
	0.346	-0.91
	0.173	-1.54
Ru(bpy) ₃ ²⁺	4.01	- .96
	2.00	-1.06
	1.00	-1.24
	0.501	-1.87
Ru(NH ₃) ₆ ³⁺	9.69	-0.032
	4.84	-0.206
	1.21	-0.97
	0.606	-2.05

a. Moles of redox species per ml of 5 w/o Nafion solution.

b. vs. SnO₂ conducting glass counter electrode.